Nonlinear Dynamics

Symmetry breaking and chaos induced imbalance in planetary gears

--Manuscript Draft--

Manuscript Number:	NODY-D-14-00757R2
Full Title:	Symmetry breaking and chaos induced imbalance in planetary gears
Article Type:	Original Research
Keywords:	Planetary gears, nonlinear vibrations, chaos
Corresponding Author:	Francesco Pellicano ITALY
Corresponding Author Secondary Information:	
Corresponding Author's Institution:	
Corresponding Author's Secondary Institution:	
First Author:	Asma Masoumi, PhD
First Author Secondary Information:	
Order of Authors:	Asma Masoumi, PhD
	Francesco Pellicano
	Farhad S. Samani, PhD
	Marco Barbieri, PhD
Order of Authors Secondary Information:	
Abstract:	The goal of the present paper is a complete analysis of the dynamic scenario of planetary gears. A lumped mass two dimensional model is adopted; the model takes into account: time varying stiffness; nonsmooth nonlinearity due to the backlash, i.e. teeth contact loosing; bearing compliance. The time varying meshing stiffness is evaluated by means of a nonlinear finite element model, which allows an accurate evaluation of global and local teeth deformation. The dynamic model is validated by comparisons with the most authoritative literature: linear natural frequencies and nonlinear response. The dynamic scenario is analyzed over a reasonable engineering range in terms of rotation speed and torque. The classical amplitude-frequency diagrams are accompanied by bifurcation diagrams and, for specific regimes, the spectral and topological properties of the response are discussed. Periodic, quasiperiodic and chaotic regimes are found, nonsmooth bifurcations lead period one to period two trajectories. It is found that the bearing compliance can influence the natural frequencies combination magnifying the modal interactions due to internal resonances and greatly enlarging the chaotic regions. It is evidenced that the chaotic response indices a symmetry breaking in the dynamical systems. The physical consequence is that the planetary gearbox under investigation, which is perfectly balanced for each position, can suffer of a big dynamic imbalance when chaotic regimes take place; such imbalance gives rise to alternate and unexpected high level stresses on bearings.
Response to Reviewers:	We followed the reviewer's suggestions, making the introduction more condensed and coherent with the journal style.

Symmetry breaking and chaos induced imbalance in planetary gears

Authors

Asma Masoumi
Department of Engineering “Enzo Ferrari”
University of Modena and Reggio Emilia, Modena, Italy
Email: asma.masoumi@gmail.com

Francesco Pellicano
Department of Engineering “Enzo Ferrari”
University of Modena and Reggio Emilia, Modena, Italy
Email: francesco.pellicano@unimore.it

Farhad S. Samani
Department of Mechanical Engineering
Shahid Bahonar University of Kerman, Kerman, Iran
Email: farhad.samani@uk.ac.ir

Marco Barbieri
Department of Engineering “Enzo Ferrari”
University of Modena and Reggio Emilia, Modena, Italy
Email: mark@unimore.it

N. of Pages 38
N. of Figures 11
N. of Tables 9

Corresponding author

Francesco Pellicano
Department of Engineering “Enzo Ferrari”
University of Modena and Reggio Emilia,
Via P. Vivarelli 10/1
41125 Modena, Italy
Email: francesco.pellicano@unimore.it
Phone: +39 0592056154
Fax: +39 0592056126

Keywords: Planetary gears, nonlinear vibrations, chaos

Abstract

The goal of the present paper is a complete analysis of the dynamic scenario of planetary gears. A lumped mass two dimensional model is adopted; the model takes into account: time varying stiffness; nonsmooth nonlinearity due to the backlash, i.e. teeth contact loosing; bearing compliance. The time varying meshing stiffness is evaluated by means of a nonlinear finite element model, which allows an accurate evaluation of global and local teeth deformation. The dynamic model is validated by comparisons with the most authoritative literature: linear natural frequencies and nonlinear response.

The dynamic scenario is analyzed over a reasonable engineering range in terms of rotation speed and torque. The classical amplitude-frequency diagrams are accompanied by bifurcation diagrams and, for specific regimes, the spectral and topological properties of the response are discussed. Periodic, quasiperiodic and chaotic regimes are found, nonsmooth bifurcations lead period one to period two trajectories. It is found that the bearing compliance can influence the natural frequencies combination magnifying the modal interactions due to internal resonances and greatly enlarging the chaotic regions.

It is evidenced that the chaotic response indices a symmetry breaking in the dynamical systems. The physical consequence is that the planetary gearbox under investigation, which is perfectly balanced for each position, can suffer of a big dynamic imbalance when chaotic regimes take place; such imbalance gives rise to alternate and unexpected high level stresses on bearings.

List of Symbols

Notation	Definition	Unit
x,y	x, y- translational coordinate	µm
Θ	Rotational coordinate	rad
k_s	Translational sun bearing-stiffness (equal for x,y)	N/m
Ψ_n	Angular position of the n^{th}-planet with respect to the x-axis	rad
α_s	Working pressure angle for sun-planet mesh	rad
α_r	Working pressure angle for planet-ring mesh	rad
$r_{bs,}r_{bn,}r_{br}$	Base radii of (sun, n^{th}-planet, ring)	m
k_{sn}	Mesh-stiffness of sun- n^{th}-planet	N/m
k_{su}	Torsional sun bearing-stiffness	N×m/rad
k_r	Translational ring bearing-stiffness (equal for x,y)	N/m
k_{rn}	Mesh-stiffness of n^{th}-planet-ring	N/m
r_c	Carrier radius (sun-planet center distance)	m
k_p	Translational planet bearing-stiffness (equal for x,y)	N/m
k_{pu}	Rotational planet bearing-stiffness (In this paper k_{pu}=0)	N×m/rad
k_c	Translational carrier bearing-stiffness (equal for x,y)	N/m
k_{cu}	Rotational carrier bearing-stiffness	N×m/rad
M_s	Sun mass	kg
θ_s	Rotational coordinate of sun	rad
C_s	Translational sun bearing-damping (equal for x,y)	N×s/m
C_{sn}	Mesh-damping of sun- n^{th}-planet	N×s/m
b_s	Sun-planet backlash	m
I_s	Sun moment of Inertia	kg×m^2
C_{su}	Torsional sun bearing-damping	N×m×s/rad
M_r	Ring mass	kg
θ_r	Rotational coordinate of ring	rad
C_r	Translational ring bearing-damping (equal for x,y)	N×s/m
C_{rn}	Mesh-damping of n^{th}-planet-ring	N×s/m
ρ_i	Dimensionless damping for the i-th mode	
b_r	Planet-ring backlash	m
I_r	Ring moment of Inertia	kg×m^2
C_{ru}	Torsional ring bearing-damping	N×m×s/rad
z	Gear numbers of teeth	
Indices:		
S	Sun	
N	n^{th}-planet	
C	Carrier	
R	Ring (Annulus)	

1. Introduction

Planetary or epicyclic gear trains are widely used in many automotive, aerospace and marine applications; they are effective power transmission systems when high torque to weight ratios, large speed reductions in compact volumes, co-axial shaft arrangements, high reliability and superior efficiency are required [1]. Gear vibrations are primary concerns in most planetary gear transmission applications, where the manifest problem may be noise or dynamic forces. The most important source of vibration in planetary gears is the parametric excitation due to the periodically time-varying mesh stiffness of each sun-planet and ring-planet gear, because the number of tooth pairs in contact changes during gear rotation. This mesh stiffness variation parametrically excites the planetary gear system, causing severe vibrations when a harmonic component approaches one of the natural frequencies (or their linear combinations). Under certain near resonant operating conditions, gear systems can experience a teeth separation that induces nonlinear effects such as jump phenomena and subharmonic and superharmonic resonances with dramatic effects on the dynamic response [2]. These phenomena have been deeply investigated in geared systems during the last 20 years [3-7].

Cunliffe et al. [8], Botman [9] and Kahraman [10–12] presented models to estimate the natural frequencies, vibration modes and dynamic forces of planetary gears. Ambarisha and Parker [1] validated the effectiveness of a lumped-parameter model to simulate the dynamics of planetary gears. In Ref. [1], responses from the dynamic analysis using analytical and finite element models are successfully compared qualitatively and quantitatively.

Multiple degrees-of-freedom linear planetary gear models are investigated in [13-15]. In such models, the gear mesh stiffness is modeled as a linear time-varying spring, [16-18].

Parker and Lin [19] found that the mesh phasing has a dramatic influence on the static and dynamic behavior of planetary and epicyclic gears. Linear system analysis helps to understand resonances and parametric instabilities due to periodically varying gear mesh stiffness [20], mesh phasing [19,20], and properties of vibration modes [14,15,23,24].

Some researchers considered two stage planetary systems [24,25]. Guo and Parker [26] derived important relations among the relative phases between any two gear meshes in a compound planetary gear.

Al-shyyab and Kahraman [27] solved the non-linear equations of planetary gear motion semi-analytically using multi-term harmonic balance method (HBM) in conjunction with inverse discrete Fourier transform and Newton–Rapson method. The nonlinear dynamics of planetary gears involving teeth wedging and bearing clearance was investigated by Guo and Parker [28]. Sun and Hu [29] investigated the nonlinear dynamics of a planetary gear system with multiple clearances; the theoretical results from HBM are verified by using the numerical integration. When the planetary gearbox operates under some inappropriate conditions, such as inadequate lubrication, poor specifications, material defects, and improper manufacturing or installation, it is likely to cause gear teeth faults. Once the tooth faults appear, the dynamic performances of the gearbox are bound to be affected, with undesirable changes in the dynamic behavior and serious reduction in the service life of the planetary system [30-33]. Recently, Gu and Velex developed a dynamic model including three dimensional effects and errors [34-35]; Li et al. proposed a deep investigation on chaotic effects in planetary gears [36].

This paper presents a dynamic model to simulate the dynamic behavior of a single-stage planetary gear system with time varying mesh stiffness and backlash. The complex dynamic scenario of a three-planets gearbox is investigated in detail. A bifurcation analysis is performed to explore the dynamic scenario (periodic, quasiperiodic and chaotic), with a special attention to symmetry breaking phenomena that are extremely interesting in planetary gears as they can cause additional imbalance-induced-stresses. Numerical analyses are carried out over meaningful mesh frequency ranges. The analysis is completed with time histories, spectra, phase portraits and Poincaré maps of the most interesting regimes.

2. Dynamical Model

The physical model of a single-stage planetary gear set is shown in Fig. 1. The system is made of four types of elements: sun gear; ring gear; N planets; carrier. Here the modeling is plane, i.e. each element has three degrees of freedom: two displacements and

a rotation. The centers of the different elements of the system are free to move in the plane, each component has translational and rotational degrees of freedom. The total number of degrees of freedom is ($3N$ + 9); the model includes time variation of gear mesh stiffness (depending on the reciprocal angular position of two meshing gears) k_{sn} and k_{rn} (n=1, 2, ..., N), backlash nonlinearities of mating gears and bearing compliance (no clearance is considered for bearings).

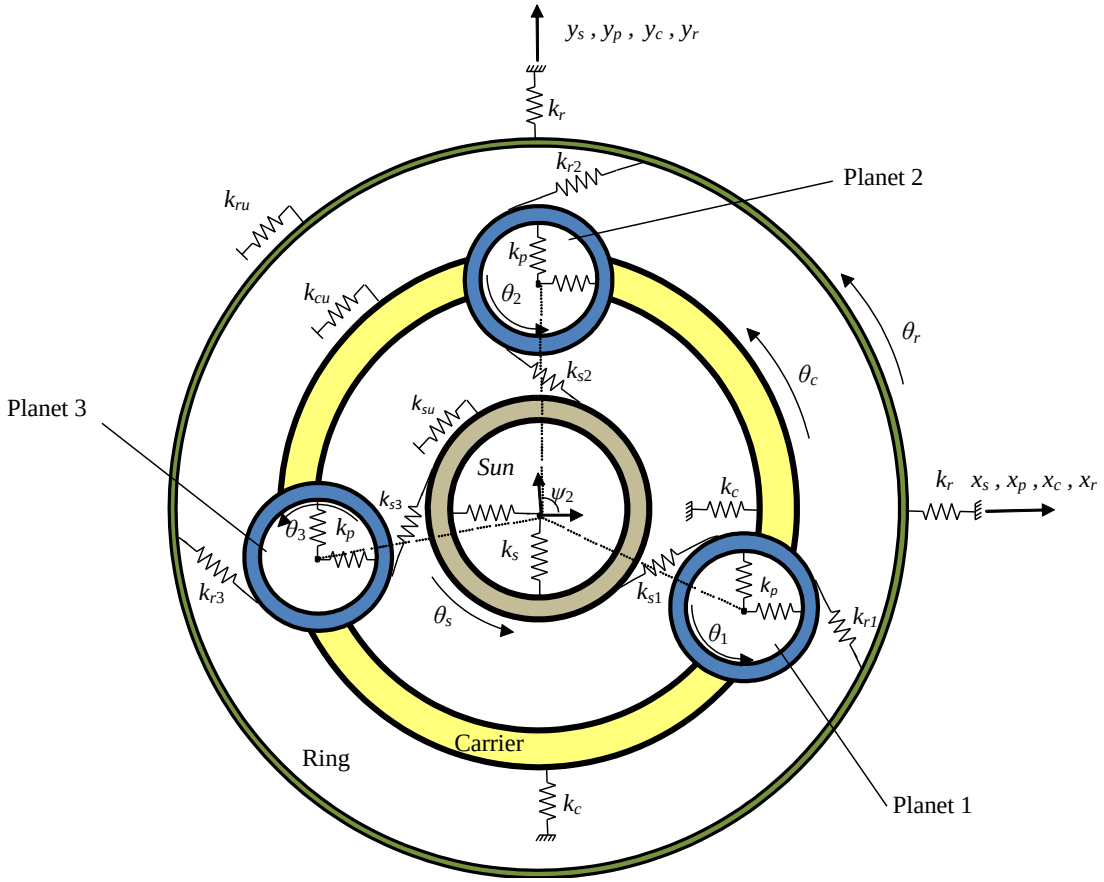

Fig. 1. Physical planar model of the single stage planetary gearbox

A single-stage planetary gear set

In Fig. 1 the planar physical model for the planetary gearbox vibration analysis is presented. Each planet is mounted on a rigid carrier through a flexible bearing; sun, ring, and carrier bearings are connected to the ground, while the planet bearings are connected

to the carrier. The planets are free to rotate with respect to the carrier; the sun is the system power input, it is also free to rotate; the rotational degree of freedom of the ring is locked; the rotation of the carrier is the system power output, it is constrained by a rotational bearing stiffness. The gear-shaft bodies, the ring and the carrier are assumed rigid; the compliant elements of the meshing gear teeth and bearings are represented by suitable nonlinear time-variant springs. The origin of the global coordinate system is at the undeflected position of the center of the sun. Positive planet position angles ψ_i (i=1, 2, ..., N) are measured counter-clockwise from the first planet, i.e. ψ_1=0, see Fig. 1.

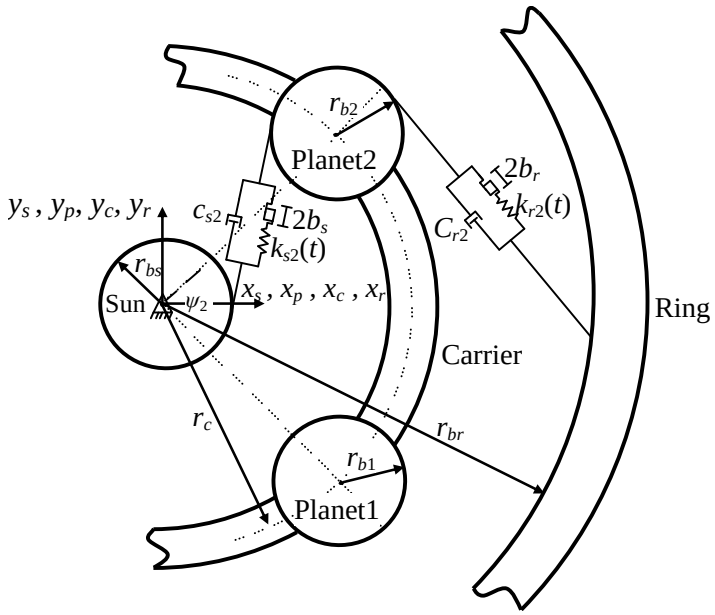

Fig. 2. Details of the meshing modeling

Details of the single-stage planetary gear set model

The gear elements, *S*, *R*, and *C*, are constrained to the ground by means of translational and torsional linear springs of stiffness magnitude (k_s,k_{su}), (k_r,k_{ru}) and (k_c,k_{cu}) respectively. Each spring is associated with a linear viscous damper, proportional to the mean value of stiffness and inertia, in order to simulate energy dissipation of the system. The planets are connected to the carrier by means of translational stiffness and damping. A proper choice of the magnitudes of the stiffness constraints allows to represent any different power flow scheme. Each gear body i (i= *S*,*R*, *C*, P_1, . . ., P_N) is modeled as a rigid disc of mass M_i, mass moment of inertia I_i, base radius r_{bi} and torsional displacement θ_i. Planets are located at radius r_c angular positions ψ_i; here the planets are considered equally spaced circumferentially. Excitation torque T_s is applied to the sun gear. The mesh

of sun (or ring) gear with a planet P_i is represented by a periodically time-varying stiffness element $k_{sn}(t)$ (or $k_{rn}(t)$) subjected to a piecewise linear backlash function f_s (or f_r) that includes a clearance of amplitude $2b_s$ (or $2b_r$).The vibrational dissipation of lubricated gear contacts is represented by constant viscous damper coefficients C_{sn} (or C_{rn}).

These coefficients are proportional to the mean stiffness coefficients and also to the mass of gears such that $\mathbf{C}=\alpha\mathbf{M}+\beta\mathbf{K}$, where **C**, **M** and **K** are damping, mass and stiffness matrices respectively and α and β are coefficients given by natural frequencies and modal damping ratios of the system, such that the damping ratio is $\rho_i=1/2(\alpha/\omega_i+\beta\omega_i)$ for the generic *i*-th mode.

3. Equations of Motion

The basic dynamical equilibrium equations contain (3*N*+9) nonlinear ordinary differential equations, where *N* is the number of planets; e.g. when *N*=3 they will be 18 coupled equations. The equations of motion of the model shown in Fig. 1 are written using Newton-Euler equations and they are placed in canonical form.

Sun Gear Equations

$$
\begin{aligned}
&-M_s\times\ddot{x}_s - C_s\times\dot{x}_s + \sum_{n=1}^{N}\Big[\Big(c_{sn}\left(\dot{x}_n-\dot{x}_s\right)\times\sin^2\left(\psi_n-\alpha_s\right)\Big)\\
&+\Big(-c_{sn}\left(\dot{y}_n-\dot{y}_s\right)\times\sin\left(\psi_n-\alpha_s\right)\times\cos\left(\psi_n-\alpha_s\right)\Big)\\
&+\Big(c_{sn}\left(\dot{\theta}_s\times r_{bs}+\dot{\theta}_n\times r_{bn}\right)\times\sin\left(\psi_n-\alpha_s\right)\Big)\Big] \qquad (1a)\\
&-k_s\times x_s + \sum_{n=1}^{N}\Big[\Big(k_{sn}\left(f_{sx}\right)\times\sin^2\left(\psi_n-\alpha_s\right)\Big)\\
&+\Big(-k_{sn}\left(f_{sy}\right)\times\sin\left(\psi_n-\alpha_s\right)\times\cos\left(\psi_n-\alpha_s\right)\Big)+\Big(k_{sn}\left(f_{s\theta}\right)\times\sin\left(\psi_n-\alpha_s\right)\Big)\Big]=0
\end{aligned}
$$

$$
\begin{aligned}
&-M_s \times \ddot{y}_s - C_s \times \dot{y}_s + \sum_{n=1}^{N}\Big[(-c_{sn}\left(\dot{x}_n - \dot{x}_s\right)\times \sin\left(\psi_n - \alpha_s\right)\times \cos(\psi_n - \alpha_s) \\
&+\left(c_{sn}\left(\dot{y}_n - \dot{y}_s\right)\times \cos^2\left(\psi_n - \alpha_s\right)\right)+\left(-c_{sn}\left(\dot{\theta}_s \times r_{bs} + \dot{\theta}_n \times r_{bn}\right)\times \cos\left(\psi_n - \alpha_s\right)\right)\Big] \\
&-k_s \times y_s + \sum_{n=1}^{N}\Big[\left(-k_{sn}\left(f_{sx}\right)\times \sin\left(\psi_n - \alpha_s\right)\times \cos(\psi_n - \alpha_s)\right) \\
&+\left(k_{sn}\left(f_{sy}\right)\times \cos^2\left(\psi_n - \alpha_s\right)\right)+\left(-k_{sn}\left(f_{s\theta}\right)\times \cos\left(\psi_n - \alpha_s\right)\right)\Big] = 0
\end{aligned}
\tag{1b}
$$

$$
\begin{aligned}
&T_s - I_s \times \ddot{\theta}_s - C_{su} \times \dot{\theta}_s + \sum_{n=1}^{N}\Big[\left(-c_{sn}\left(\dot{x}_n - \dot{x}_s\right)\times \sin\left(\psi_n - \alpha_s\right)\times r_{bs}\right) \\
&+\left(c_{sn}\left(\dot{y}_n - \dot{y}_s\right)\times \cos\left(\psi_n - \alpha_s\right)\times r_{bs}\right)+\left(-c_{sn}\left(\dot{\theta}_s \times r_{bs} + \dot{\theta}_n \times r_{bn}\right)\times r_{bs}\right)\Big] \\
&-k_{su} \times \theta_s + \sum_{n=1}^{N}\Big[\left(-k_{sn}\left(f_{sx}\right)\times \sin\left(\psi_n - \alpha_s\right)\times r_{bs}\right) \\
&+\left(k_{sn}\left(f_{sy}\right)\times \cos\left(\psi_n - \alpha_s\right)\times r_{bs}\right)+\left(-k_{sn}\left(f_{s\theta}\right)\times r_{bs}\right)\Big] = 0
\end{aligned}
\tag{1c}
$$

In these equations, x and y and θ are the translational and rotational degrees of freedom respectively. T_s is the constant input torque applied to the sun gear and f_{sx}, f_{sy} and $f_{s\theta}$ are the piecewise-linear displacement functions for sun-planets meshing, which are defined as follows:

$$
f_{sx} = \begin{cases}
x_n - x_s - \dfrac{b_s}{\sin\left(\psi_n - \alpha_s\right)} & \Delta_{sn} \geq b_s \\
0 & \left|\Delta_{sn}\right| < b_s \\
x_n - x_s + \dfrac{b_s}{\sin\left(\psi_n - \alpha_s\right)} & \Delta_{sn} \leq -b_s
\end{cases}
\tag{2a}
$$

$$
f_{sy} = \begin{cases}
y_n - y_s + \dfrac{b_s}{\cos(\psi_n - \alpha_s)} & \Delta_{sn} \geq b_s \\
0 & \left|\Delta_{sn}\right| < b_s \\
y_n - y_s - \dfrac{b_s}{\cos(\psi_n - \alpha_s)} & \Delta_{sn} \leq -b_s
\end{cases}
\tag{2b}
$$

$$f_{s\theta}=\begin{cases}\theta_s\times r_{bs}+\theta_n\times r_{bn}-b_s & \Delta_{sn}\geq b_s\\ 0 & |\Delta_{sn}|<b_s\\ \theta_s\times r_{bs}+\theta_n\times r_{bn}+b_s & \Delta_{sn}\leq -b_s\end{cases} \quad (2c)$$

where,

$$\Delta_{sn}=\left[\left(x_n-x_s\right)\times\sin(\psi_n-\alpha_s)-\left(y_n-y_s\right)\times\cos(\psi_n-\alpha_s)+\left(\theta_s\times r_{bs}+\theta_n\times r_{bn}\right)\right] \quad (3)$$

When $|\Delta_{sn}|<b_s$ the teeth are separated, when $\Delta_{sn}\leq -b_s$ backside contact occurs.

Ring Gear Equations

$$\begin{aligned}&-M_r\times\ddot{x}_r-C_r\times\dot{x}_r+\sum_{n=1}^{N}\left[\left(-c_{rn}\left(\dot{x}_r-\dot{x}_n\right)\times\sin^2\left(\psi_n+\alpha_r\right)\right)\right.\\&\left.+\left(c_{rn}\left(\dot{y}_r-\dot{y}_n\right)\times\sin\left(\psi_n+\alpha_r\right)\times\cos(\psi_n+\alpha_r)\right)+\left(c_{rn}\left(\dot{\theta}_r\times r_{br}-\dot{\theta}_n\times r_{bn}\right)\times\sin\left(\psi_n+\alpha_r\right)\right)\right]\\&-k_r\times x_r+\sum_{n=1}^{N}\left[\left(-k_{rn}\left(f_{rx}\right)\times\sin^2\left(\psi_n+\alpha_r\right)\right)+\left(k_{rn}\left(f_{ry}\right)\times\sin\left(\psi_n+\alpha_r\right)\times\cos(\psi_n+\alpha_r)\right)\right.\\&\left.+\left(k_{rn}\left(f_{r\theta}\right)\times\sin\left(\psi_n+\alpha_r\right)\right)\right]=0\end{aligned} \quad (4a)$$

$$\begin{aligned}&-M_r\times\ddot{y}_r-C_r\times\dot{y}_r+\sum_{n=1}^{N}\left[\left(k_{rn}\left(x_r-x_n\right)\times\sin\left(\psi_n+\alpha_r\right)\times\cos(\psi_n+\alpha_r)\right)\right.\\&\left.+\left(-k_{rn}\left(y_r-y_n\right)\times\cos^2(\psi_n+\alpha_r)\right)+\left(-k_{rn}\left(\theta_r\times r_{br}-\theta_n\times r_{bn}\right)\times\cos\left(\psi_n+\alpha_r\right)\right)\right]\\&-k_r\times y_r+\sum_{n=1}^{N}\left[\left(k_{rn}\left(f_{rx}\right)\times\sin\left(\psi_n+\alpha_r\right)\times\cos(\psi_n+\alpha_r)\right)\right.\\&\left.+\left(-k_{rn}\left(f_{ry}\right)\times\cos^2(\psi_n+\alpha_r)\right)+\left(-k_{rn}\left(f_{r\theta}\right)\times\cos\left(\psi_n+\alpha_r\right)\right)\right]=0\end{aligned} \quad (4b)$$

$$\begin{aligned}&-I_r\times\ddot{\theta}_r-C_{ru}\times\dot{\theta}_r+\sum_{n=1}^{N}\left[\left(c_{rn}\left(\dot{x}_r-\dot{x}_n\right)\times\sin\left(\psi_n+\alpha_r\right)\times r_{br}\right)\right.\\&\left.+\left(-c_{rn}\left(\dot{y}_r-\dot{y}_n\right)\times\cos(\psi_n+\alpha_r)\times r_{br}\right)+\left(-c_{rn}\left(\dot{\theta}_r\times r_{br}-\dot{\theta}_n\times r_{bn}\right)\times r_{br}\right)\right]\\&-k_{ru}\times\theta_r+\sum_{n=1}^{N}\left[\left(k_{rn}\left(f_{rx}\right)\times\sin\left(\psi_n+\alpha_r\right)\times r_{br}\right)\right.\\&\left.+\left(-k_{rn}\left(f_{ry}\right)\times\cos(\psi_n+\alpha_r).r_{br}\right)+\left(-k_{rn}\left(f_{r\theta}\right)\times r_{br}\right)\right]=0\end{aligned} \quad (4c)$$

where, f_{rx}, f_{ry} and $f_{r\theta}$ are the following:

$$f_{rx}=\begin{cases} x_r - x_n + \dfrac{b_r}{\sin(\psi_n+\alpha_r)} & \Delta_{rn} \ge b_r \\ 0 & |\Delta_{rn}| < b_r \\ x_r - x_n - \dfrac{b_r}{\sin(\psi_n+\alpha_r)} & \Delta_{rn} \le -b_r \end{cases} \quad (5a)$$

$$f_{ry}=\begin{cases} y_r - y_n - \dfrac{b_r}{\cos(\psi_n+\alpha_r)} & \Delta_{rn} \ge b_r \\ 0 & |\Delta_{rn}| < b_r \\ y_r - y_n + \dfrac{b_r}{\cos(\psi_n+\alpha_r)} & \Delta_{rn} \le -b_r \end{cases} \quad (5b)$$

$$f_{r\theta}=\begin{cases} \theta_r \times r_{br} - \theta_n \times r_{bn} - b_r & \Delta_{rn} \ge b_r \\ 0 & |\Delta_{rn}| < b_r \\ \theta_r \times r_{br} - \theta_n \times r_{bn} + b_r & \Delta_{rn} \le -b_r \end{cases} \quad (5c)$$

and

$$\Delta_{rn}=\left[-\left(x_r-x_n\right)\times\sin(\psi_n+\alpha_r)+\left(y_r-y_n\right)\times\cos(\psi_n+\alpha_r)+\left(\theta_r\times r_{br}-\theta_n\times r_{bn}\right)\right] \quad (6)$$

Similarly to the sun-planet contact, tooth-separation occurs when $|\Delta_{rn}| < b_r$, while if $\Delta_{rn} \le -b_r$ the contact is on the opposite flank.

Planets Gear Equations

$$\begin{aligned} &-M_p\times\ddot{x}_n - C_p\times\left(\dot{x}_n-\dot{x}_c+r_c\dot{\theta}_c\times\sin\left(\psi_n\right)\right)+\left(-c_{sn}\left(\dot{x}_n-\dot{x}_s\right)\times\sin^2\left(\psi_n-\alpha_s\right)\right) \\ &+\left(c_{rn}\left(\dot{x}_r-\dot{x}_n\right)\times\sin^2\left(\psi_n+\alpha_r\right)\right)+\left(c_{sn}\left(\dot{y}_n-\dot{y}_s\right)\times\sin\left(\psi_n-\alpha_s\right)\times\cos\left(\psi_n-\alpha_s\right)\right) \\ &+\left(-c_{rn}\left(\dot{y}_r-\dot{y}_n\right)\times\sin\left(\psi_n+\alpha_r\right)\times\cos\left(\psi_n+\alpha_r\right)\right)+\left(-c_{sn}\left(\dot{\theta}_s\times r_{bs}+\dot{\theta}_n\times r_{bn}\right)\times\sin\left(\psi_n-\alpha_s\right)\right) \\ &+\left(-c_{rn}\left(\dot{\theta}_r.\times r_{br}-\dot{\theta}_n\times r_{bn}\right)\times\sin\left(\psi_n+\alpha_r\right)\right)-k_p\times\left(x_n-x_c+r_c\theta_c\sin\left(\psi_n\right)\right) \\ &+\left(-k_{sn}\left(f_{sx}\right)\times\sin^2\left(\psi_n-\alpha_s\right)\right)+\left(k_{rn}\left(f_{rx}\right)\times\sin^2\left(\psi_n+\alpha_r\right)\right) \\ &+\left(k_{sn}\left(f_{sy}\right)\times\sin\left(\psi_n-\alpha_s\right)\times\cos\left(\psi_n-\alpha_s\right)\right)+\left(-k_{rn}\left(f_{ry}\right)\times\sin\left(\psi_n+\alpha_r\right)\times\cos\left(\psi_n+\alpha_r\right)\right) \\ &+\left(-k_{sn}\left(f_{s\theta}\right)\times\sin\left(\psi_n-\alpha_s\right)\right)+\left(-k_{rn}\left(f_{r\theta}\right)\times\sin\left(\psi_n+\alpha_r\right)\right)=0 \end{aligned}$$

(7a)

$$
\begin{aligned}
&-M_p \times \ddot{y}_n - C_p \times \left(\dot{y}_n - \dot{y}_c - r_c\dot{\theta}_c \cos\left(\psi_n\right)\right) + \left(c_{sn}\left(\dot{x}_n - \dot{x}_s\right) \times \sin\left(\psi_n - \alpha_s\right) \times \cos(\psi_n - \alpha_s)\right) \\
&+ \left(-c_{rn}\left(\dot{x}_r - \dot{x}_n\right) \times \sin\left(\psi_n + \alpha_r\right) \times \cos(\psi_n + \alpha_r)\right) + \left(-c_{sn}\left(\dot{y}_n - \dot{y}_s\right) \times \cos^2\left(\psi_n - \alpha_s\right)\right) \\
&+ \left(c_{rn}\left(\dot{y}_r - \dot{y}_n\right) \times \cos^2(\psi_n + \alpha_r)\right) + \left(c_{sn}\left(\dot{\theta}_s \times r_{bs} + \dot{\theta}_n \times r_{bn}\right) \times \cos\left(\psi_n - \alpha_s\right)\right) \\
&+ \left(c_{rn}\left(\dot{\theta}_r \times r_{br} - \dot{\theta}_n \times r_{bn}\right) \times \cos\left(\psi_n + \alpha_r\right)\right) - k_p \times \left(y_n - y_c - r_c\theta_c \cos\left(\psi_n\right)\right) \\
&+ \left(k_{sn}\left(f_{sx}\right) \times \sin\left(\psi_n - \alpha_s\right) \times \cos(\psi_n - \alpha_s)\right) + \left(-k_{rn}\left(f_{rx}\right) \times \sin\left(\psi_n + \alpha_r\right) \times \cos(\psi_n + \alpha_r)\right) \\
&+ \left(-k_{sn}\left(f_{sy}\right) \times \cos^2\left(\psi_n - \alpha_s\right)\right) + \left(k_{rn}\left(f_{ry}\right) \times \cos^2(\psi_n + \alpha_r)\right) \\
&+ \left(k_{sn}\left(f_{s\theta}\right) \times \cos\left(\psi_n - \alpha_s\right)\right) + \left(k_{rn}\left(f_{r\theta}\right) \times \cos\left(\psi_n + \alpha_r\right)\right) = 0
\end{aligned}
$$

(7b)

$$
\begin{aligned}
&-I_p \times \ddot{\theta}_n + \left(-c_{sn}\left(\dot{x}_n - \dot{x}_s\right) \times \sin\left(\psi_n - \alpha_s\right) \times r_{bn}\right) + \left(-c_{rn}\left(\dot{x}_r - \dot{x}_n\right) \times \sin\left(\psi_n + \alpha_r\right) \times r_{bn}\right) \\
&+ \left(c_{sn}\left(\dot{y}_n - \dot{y}_s\right) \times \cos\left(\psi_n - \alpha_s\right) \times r_{bn}\right) + \left(c_{rn}\left(\dot{y}_r - \dot{y}_n\right) \times \cos(\psi_n + \alpha_r) \times r_{bn}\right) \\
&+ \left(-c_{sn}\left(\dot{\theta}_s \times r_{bs} + \dot{\theta}_n \times r_{bn}\right) \times r_{bn}\right) + \left(c_{rn}\left(\dot{\theta}_r \times r_{br} - \dot{\theta}_n \times r_{bn}\right) \times r_{bn}\right) + \left(-k_{sn}\left(f_{sx}\right) \times \sin\left(\psi_n - \alpha_s\right) \times r_{bn}\right) \\
&+ \left(-k_{rn}\left(f_{rx}\right) \times \sin\left(\psi_n + \alpha_r\right) \times r_{bn}\right) + \left(k_{sn}\left(f_{sy}\right) \times \cos\left(\psi_n - \alpha_s\right) \times r_{bn}\right) \\
&+ \left(k_{rn}\left(f_{ry}\right) \times \cos(\psi_n + \alpha_r) \times r_{bn}\right) + \left(-k_{sn}\left(f_{s\theta}\right) \times r_{bn}\right) + \left(k_{rn}\left(f_{r\theta}\right) \times r_{bn}\right) = 0
\end{aligned}
$$

(7c)

Carrier Equations

$$
\begin{aligned}
&-M_c \times \ddot{x}_c - c_c \times \dot{x}_c - k_c \times x_c + \sum_{n=1}^{N}\left[c_p \times \left(\dot{x}_n - \dot{x}_c + r_c\dot{\theta}_c \sin\left(\psi_n\right)\right)\right] \\
&+ \sum_{n=1}^{N}\left[k_p \times \left(x_n - x_c + r_c\theta_c \sin\left(\psi_n\right)\right)\right] = 0
\end{aligned}
$$

(8a)

$$
\begin{aligned}
&-M_c \times \ddot{y}_c - c_c \times \dot{y}_c - k_c \times y_c + \sum_{n=1}^{N}\left[c_p \times \left(\dot{y}_n - \dot{y}_c - r_c\dot{\theta}_c \cos\left(\psi_n\right)\right)\right] \\
&+ \sum_{n=1}^{N}\left[k_p \times \left(y_n - y_c - r_c\theta_c \cos\left(\psi_n\right)\right)\right] = 0
\end{aligned}
$$

(8b)

$$-I_c \times \ddot{\theta}_c - c_{cu} \times \dot{\theta}_c - k_{cu} \times \theta_c + \sum_{n=1}^{N}\left[\left(-c_p \times \left(\dot{x}_n - \dot{x}_c + r_c\dot{\theta}_c \sin\left(\psi_n\right)\right) \times r_c \sin\left(\psi_n\right)\right)\right.$$
$$\left.+\left(c_p \times \left(\dot{y}_n - \dot{y}_c - r_c\dot{\theta}_c \cos\left(\psi_n\right)\right) \times r_c \cos\left(\psi_n\right)\right)\right]$$
$$+\sum_{n=1}^{N}\left[\left(-k_p \times \left(x_n - x_c + r_c\theta_c \sin\left(\psi_n\right)\right) \times r_c \sin\left(\psi_n\right)\right)\right.$$
$$\left.+\left(k_p \times \left(y_n - y_c - r_c\theta_c \cos\left(\psi_n\right)\right) \times r_c \cos\left(\psi_n\right)\right)\right] = 0 \qquad (8c)$$

In the equations (1-8), $k_{sn}(t)$ and $k_{rn}(t)$ are the mesh stiffnesses between sun-planet and ring-planet gears, respectively; they are periodically time varying at the mesh frequency. As the number of teeth pairs in contact within the mesh cycle changes with the rotation of the gear, the mesh stiffness varies accordingly. The piecewise linear spring generates nonzero mesh force only for positive relative mesh deflection (teeth in contact). The combination of the static torque and time varying stiffness gives rise to the excitation of the system, the periodic stiffness has the fundamental frequency $\omega_m = \omega_s z_s z_r / (z_s + z_r)$ where ω_s is the angular velocity of the sun gear and z_s and z_r are the teeth numbers of the sun and the ring gears. Periodically time-varying mesh stiffnesses are written in Fourier series form:

$$k_{sn}(t) = k_{sp}^1 + \sum_{n=1}^{h_s}\left(k_{sp}^{2n} \times \cos\left(\omega_m \times t - 2\gamma_{sn} \times \pi\right) + k_{sp}^{(2n+1)} \times \sin\left(\omega_m \times t - 2\gamma_{sn} \times \pi\right)\right) \qquad (9a)$$

$$k_{rn}(t) = k_{rp}^1 + \sum_{n=1}^{h_r}\left(k_{rp}^{2n} \times \cos(\omega_m \times t - 2\hat{\gamma}_{rn} \times \pi) + k_{rp}^{2n+1} \times \sin(\omega_m \times t - 2\hat{\gamma}_{rn} \times \pi)\right) \qquad (9b)$$

Where h_s and h_r are the number of harmonic terms used to describe the periodic functions $k_{sn}(t)$ and $k_{rn}(t)$; $k_{sp}^{(i)}$ and $k_{rp}^{(i)}$ are the harmonic coefficients of Fourier series. $k_{sp}^{(1)}$ and $k_{rp}^{(1)}$ are the mean values of the coefficients; γ_{sn} represents the phasing between sun-planets, which means relative phase between n^{th} sun-planet mesh and first sun-planet mesh, i.e. $\gamma_{s1} = 0$; the same definition applies to $\hat{\gamma}_{rn}$, which is relative phase between n^{th} ring-planet mesh and first ring-planet mesh, $\hat{\gamma}_{rn} = \gamma_{sn} + \gamma_{sr}$ represents the ring-planets phasing; γ_{sr} is the sun-ring phasing i.e. the phase angle between the n^{th} ring-planet mesh and the n^{th} sun-planet mesh. For the present study, γ_{sr} is independent from planet number;

so, γ_{sr} is phase angle between stiffnesses of meshes sun-first planet and ring-first planet. See Ref. [21] for a comprehensive description on mesh phase relations in planetary gears.

4. Time-varying mesh stiffness evaluation

The gear meshes are considered as linear springs with backlash (nonlinearity) and periodically varying stiffness, due to the variation of tooth contact conditions and position of contact points on each tooth. This time varying mesh stiffness is evaluated by *HelicalPair* software [11, 38]. *HelicalPair* is a software developed in the Centre Intermech MO.RE. (Aster, High Technology Network of the Emilia Romagna Region). Linearized gear mesh stiffness (without considering backlash effects) is evaluated separately both for external gears (sun-planets mesh) and internal gears (ring-planets mesh). *HelicalPair* acts as a preprocessor and postprocessor for a FE solver, namely MSC Marc software. Figs. 3a and 3b illustrate finite element model produced by *HelicalPair* software for external and internal gear meshes. Figs. 3c and 3d present details of gear tooth meshes; backlashes are observable in these figures.

The mesh stiffnesses are dependent on the forcing condition (torque applied). For external gear meshes, the torque $T_s=T/N$ is applied to the sun, where T is the sun torque of the planetary system, the transmission error is calculated using *HelicalPair* ($u_s=r_s\theta_s$), the mesh stiffness $\hat{k}_{s1}$ at a particular mesh position is evaluated as $\hat{k}_{s1}=T_s/(r_s u_s)$. This calculation is repeated at multiple steps within a mesh cycle. A similar process is used for the ring–planet mesh; the torque $T_p=T_s z_p/z_s$ is applied to the planet. In each case, the center of the driven gear is fixed when the stiffness is evaluated.

Note that the present calculations of the applied torques are valid when the load is uniformly distributed among different planets (balanced gearbox). In actual gearboxes, it is impossible to guarantee uniform loading when more than three planets are present, due to the quality accuracy of workmanship [33].

(a) (b)

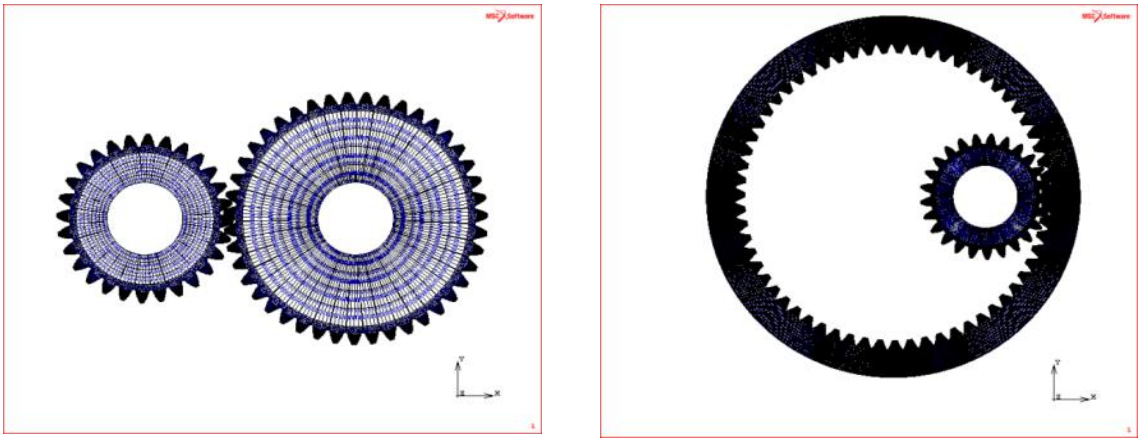

(c) (d)

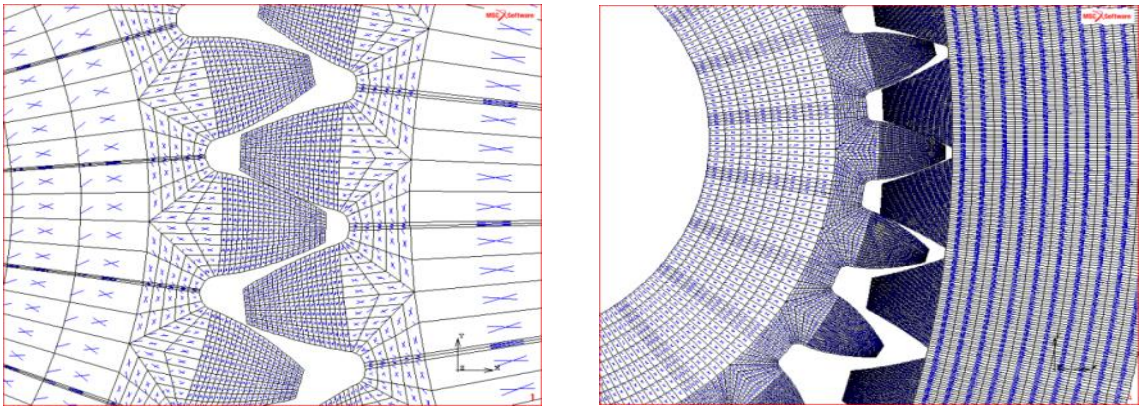

Fig. 3 Finite element model gear meshes: a: external gears, b: internal gears, c: external gear teeth meshes, d: internal gear teeth meshes.

5. Validation

First Validation: Pure Rotational Model

In this section, the results are validated by comparisons with Ref. [2], where a pure rotational nonlinear model was considered. The gear tooth flanks are pure involutes without tooth modification. The parameters of the gearbox are given in Table 1. The gearbox is made of three equally spaced planets, i.e. N=3 and ψ_i = 0, 2π/3, 4π/3. The half backlash values for both meshes are b_s= b_r =0.3 mm [2]. A constant sun gear torque of

1130Nm is applied. The ring gear is fixed in the present study. The carrier rotational dof θ_c is constrained to be zero under the assumption that there is a large output inertia (as usual for many applications), so the rigid body motion is removed [2].

The average stiffness values of the sun–planet and ring–planet meshes are: $k_{sp}^{(1)}$=6.197×10^{8}N/m and $k_{sp}^{(1)}$=8.512×10^{8}N/m, see Ref.[2]. Stiffnesses are evaluated by Fourier coefficients given in Table 2. The values of the gear mesh damping constants $C_{sn}(t)$ (or $C_{rn}(t)$) are estimated such that they correspond to the damping ratios given in Table 3.

Table 1. Parameters of the case study planetary gear set (Rotational Model)

Parameter	Sun	Planet	Ring	Carrier
Number of teeth	27	35	99	-
Module [mm]	2.8677	2.8677	2.7782	-
Pressure angle [deg]	24.60	20.19		-
Working Center Distance [mm]		88.89		-
Root diameter [mm]	70.485	91.440	284.150	-
Outer diameter [mm]	84.074	105.004	304.800	-
Inner diameter [mm]	57.15	73.66	271.73	-
Base diameter [mm]	70.40	91.26	258.130	177.80
Translational bearing stiffness [N/m]	-	-	-	-
Rotational bearing stiffness [N.m/rad]	0	0	-	2.19e10
***I*/*r*^{2} [kg]**	3.11	4.89	-	24.80
Mass [kg]		2.64		

Table 2. Fourier coefficients of sun-planet and ring-planet mesh stiffnesses [N/m], see Eq. (9)

Harmonics (*n*)	$k_{sn}\times10^7$		$k_{rn}\times10^7$	
	k_{sp}^{2n}	k_{sp}^{2n+1}	k_{rp}^{2n}	k_{rp}^{2n+1}
1	-12.632	8.462	-0.192	2.342
2	-0.634	2.634	0.15	0.022
3	-0.702	-3.07	-0.326	0.306
4	-1.63	-1.404	0.508	0.422
5	0.392	0.04	0.446	-0.444

Table 3. Damping ratios

Low frequency range	ρ_1= 2.7%, ρ_2= ρ_3=1.1%, ρ_4=1.92%
High frequency range	ρ_1= 6%, ρ_2= ρ_3=1.1%, ρ_4=5%

All sun-planet meshes are in phase with each other, as well as all ring-planet meshes, i.e. γ_{sn}=γ_{rn}=0. This design can be realized when the summation of sun and ring teeth numbers is an integer multiple of the number of planets [2]. In the absence of chaotic responses, caused by nonlinear effects, this arrangment presents symmetric force distribution, i.e. perfect balancing on the sun (zero forces acting on the bearings).

The natural frequencies of the present model (reduced to pure rotational motion by elimination of translational degrees of freedom) are presented in the Table 4. Good agreement between Ref. [2] and the present model is found.

The nonlinear model is validated considering regimes where the amplitudes of vibration cause teeth separation, i.e. nonlinear behavior. Fig.4 shows the RMS (Root Mean Square) of sun rotational vibration (multiplied by sun base radius) vs. the meshing frequency; such results are obtained by numerical integrating Eqs.(1-8); the mean value of time histories is removed before calculating the RMS. The algorithm for numerical integration is RADAU5; the number of mesh periods considered for transient response is 950 (initial response removed from the analysis), the number of substeps is 100 per each period and the number of mesh periods considered for evaluating the RMS is 50.

The mesh frequency is dependent on the sun rotational speed by $\omega_m = z_s z_r / (z_s + z_r)\omega_s$.

Table 4. Comparison of Natural frequencies for pure rotational model			
Natural frequency	Presentresults [Hz]	Results of Ref. [2] [Hz]	The difference [%]
ω_1	1847	1846	0.05
$\omega_2 = \omega_3$	2760	2744	0.5
ω_4	4387	4379	0.18

Results for both increasing and decreasing speed sweeps are plotted in Fig. 4, only the sun rotational dof is represented for the sake of brevity. There are jump phenomena at the first (ω_1) and the fourth (ω_4) resonances. The resonance peaks lean-to the left, implying softening nonlinearity induced by tooth separation.There are additional resonance peaks around 8000 Hz,1800 Hz (the first distinct mode), and below 1600 Hz. These peaks are the combined effect of parametric instability from higher harmonics of mesh stiffness fluctuation and nonlinear subharmonic and superharmonic resonances of the first and second distinct modes, [2].

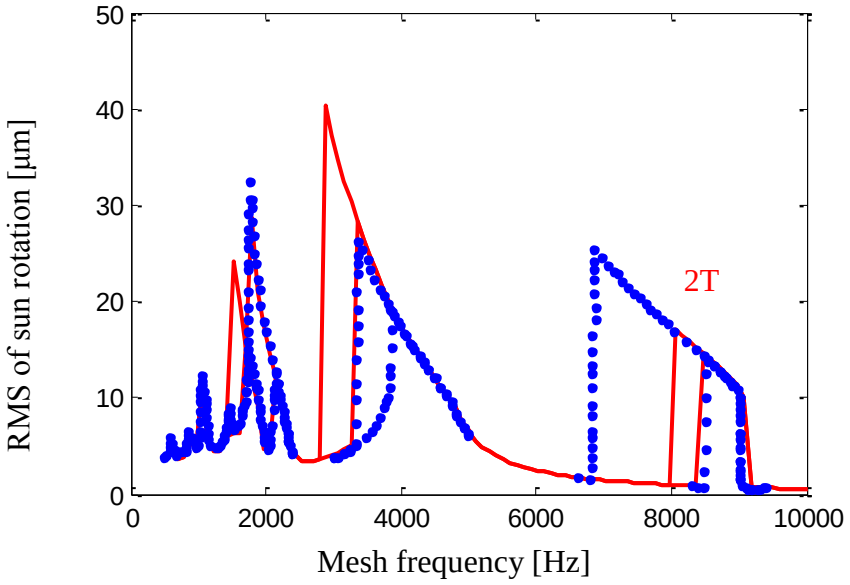

Fig. 4. RMS of sun rotation versus mesh frequency; ——: present results, ●●●: results of Ref.[2].

Second Validation: Rotational – Translational Model

The full model for nonlinear dynamics of planetary gears is investigated here using all degrees of freedom for sun, planets, carrier and ring gears. Comparison between the rotational – translational bulk model with the results of Ref. [1] is presented. The natural frequencies of both models are listed in Table 6 (gearbox data are available in Tables 2, 3 and 5) Fig 5 represents the RMS (mean removed) of sun compared for pure rotational and rotational-translational model.

The eigenvectors correlated to the natural frequencies of Table 5 are plotted in Fig. 6. These eigenvectors are normalized by unity. Table 7 presents the description of each degree of freedom. The modes (1758Hz) and (3352Hz) are related to planets rotations, the amplitudes of the other degrees of freedom are almost zero.

Table 5. Parameters of the case study planetary gear set (Rotational- translational Model)

Parameter	Sun	Planet	Ring	Carrier
Number of teeth	27	35	99	-
Module [mm]	2.8677	2.8677	2.7782	-
Pressure angle [deg]	24.60	20.19		-
Working Center Distance [mm]	88.89			-
Root diameter [mm]	70.485	91.440	284.150	-
Outer diameter [mm]	84.074	105.004	304.800	-
Inner diameter [mm]	57.15	73.66	271.73	-
Base diameter [mm]	70.40	91.26	258.130	177.80
Translational bearing stiffness [N/m]	2.19e9	2.19e9	2.19e10	2.19e10
Rotational bearing stiffness [N.m/rad]	0	0	2.19e10	2.19e10
$\boldsymbol{I/r^2}$ **[kg]**	1.56	2.46	-	24.80
Mass [kg]	1.64	1.33	-	21.82

Table 6: Comparison of Natural frequencies for rotational-translational model

Natural Freq.	Present model[Hz]	Ref. [2] [Hz]	% difference

$\omega_1 = \omega_2$	1758	1760	0.1
ω_3	2100	2095	0.19
$\omega_4 = \omega_5$	3352	3390	1.1
ω_6	5253	5249	0.07

Table 7: Definition of each degree of freedoms

1	Sun gear translation in *x* direction	**10**	2nd planet translation in *x* direction
2	Sun gear translation in *y* direction	**11**	2nd planet translation in *y* direction
3	Sun gear rotation	**12**	2nd planet gear rotation
4	Ring gear translation in *x* direction	**13**	3rd planet translation in *x* direction
5	Ring gear translation in *y* direction	**14**	3rd planet translation in *y* direction
6	Ring gear rotation	**15**	3rd planet gear rotation
7	1st planet translation in *x* direction	**16**	Carrier translation in *x* direction
8	1st planet translation in *y* direction	**17**	Carrier translation in *y* direction
9	1st planet gear rotation	**18**	Carrier gear rotation

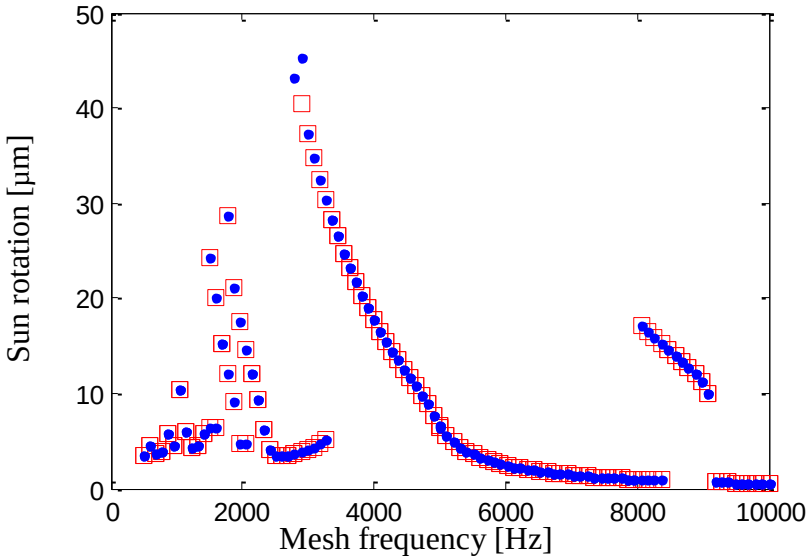

Fig.5. RMS of sun rotation;□: pure rotational model, ●: rotational translational model.

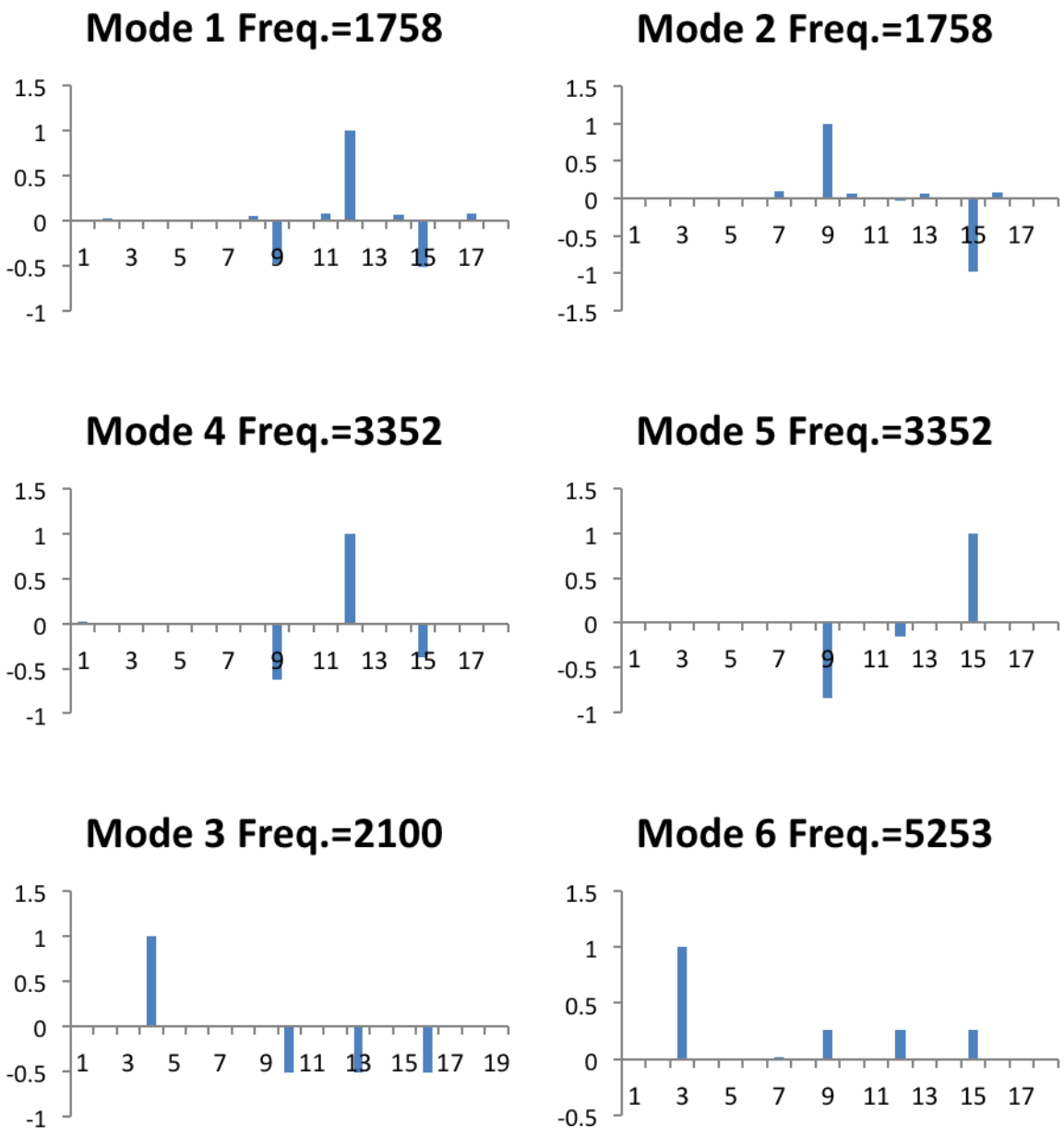

Fig.6. 6 first mode shapes of the system corresponding to Table 6. Definition of degrees of freedoms are in Table 7.